Wavefront reconstruction by modal decomposition

Christian Schulze,[1,*] Darryl Naidoo,[2] Daniel Flamm,[1] Oliver A. Schmidt,[1,3] Andrew Forbes,[2,4] and Michael Duparré[1]

[1]*Institute of Applied Optics, Fröbelstieg 1, 07743 Jena, Germany*
[2]*Council for Scientific and Industrial Research National Laser Centre, P.O. Box 395, Pretoria, South Africa*
[3]*Now with the Max Planck Institute for the Science of Light, Guenther-Scharowsky-Str. 1, 91058 Erlangen, Germany*
[4]*School of Physics, University of KwaZulu-Natal, Private Bag X54001, Durban 4000, South Africa*

[*]*christian.schulze@uni-jena.de*

Abstract: We propose a new method to determine the wavefront of a laser beam based on modal decomposition by computer-generated holograms. The hologram is encoded with a transmission function suitable for measuring the amplitudes and phases of the modes in real-time. This yields the complete information about the optical field, from which the Poynting vector and the wavefront are deduced. Two different wavefront reconstruction options are outlined: reconstruction from the phase for scalar beams, and reconstruction from the Poynting vector for inhomogeneously polarized beams. Results are compared to Shack-Hartmann measurements that serve as a reference and are shown to reproduce the wavefront and phase with very high fidelity.

OCIS codes: (140.3295) Laser beam characterization; (010.7350) Wave-front sensing; (120.5050) Phase measurement; (090.1995) Digital holography; (030.4070) Modes; (050.4865) Optical vortices.

References and links

1. F. Roddier, M. Séchaud, G. Rousset, P.-Y. Madec, M. Northcott, J.-L. Beuzit, F. Rigaut, J. Beckers, D. Sandler, P. Léna, and O. Lai, *Adaptive Optics in Astronomy* (Cambridge, 1999).
2. M. A. A. Neil, R. Jukaitis, M. J. Booth, T. Wilson, T. Tanaka, and S. Kawata, "Adaptive aberration correction in a two-photon microscope," J. Microsc. **200**, 105–108 (2000).
3. M. Rueckel, J. A. Mack-Bucher, and W. Denk, "Adaptive wavefront correction in two-photon microscopy using coherence-gated wavefront sensing," Proc. Natl. Acad. Sci. **103**, 17137–17142 (2006).
4. M. Booth, M. Neil, and T. Wilson, "Aberration correction for confocal imaging in refractive-index-mismatched media," J. Microsc. **192**, 90–98 (1998).
5. B. Hermann, E. J. Fernández, A. Unterhuber, H. Sattmann, A. F. Fercher, W. Drexler, P. M. Prieto, and P. Artal, "Adaptive-optics ultrahigh-resolution optical coherence tomography," Opt. Lett. **29**, 2142–2144 (2004).
6. A. Roorda, F. Romero-Borja, I. William Donnelly, H. Queener, T. Hebert, and M. Campbell, "Adaptive optics scanning laser ophthalmoscopy," Opt. Express **10**, 405–412 (2002).
7. R. Paschotta, *Encyclopedia of Laser Physics and Technology* (Wiley, 2008).
8. M. Paurisse, M. Hanna, F. Druon, and P. Georges, "Wavefront control of a multicore ytterbium-doped pulse fiber amplifier by digital holography," Opt. Lett. **35**, 1428–1430 (2010).
9. R. Navarro and E. Moreno-Barriuso, "Laser ray-tracing method for optical testing," Opt. Lett. **24**, 951–953 (1999).
10. S. R. Chamot, C. Dainty, and S. Esposito, "Adaptive optics for ophthalmic applications using a pyramid wavefront sensor," Opt. Express **14**, 518–526 (2006).

#171597 - $15.00 USD Received 29 Jun 2012; revised 2 Aug 2012; accepted 3 Aug 2012; published 13 Aug 2012

11. M. P. Rimmer and J. C. Wyant, "Evaluation of large aberrations using a lateral-shear interferometer having variable shear," Appl. Opt. **14**, 142–150 (1975).
12. J.-C. Chanteloup, F. Druon, M. Nantel, A. Maksimchuk, and G. Mourou, "Single-shot wave-front measurements of high-intensity ultrashort laser pulses with a three-wave interferometer," Opt. Lett. **23**, 621–623 (1998).
13. S. Velghe, J. Primot, N. Guérineau, M. Cohen, and B. Wattellier, "Wave-front reconstruction from multidirectional phasederivatives generated by multilateral shearing interferometers," Opt. Lett. **30**, 245–247 (2005).
14. R. G. Lane and M. Tallon, "Wave-front reconstruction using a Shack-Hartmann sensor," Appl. Opt. **31**, 6902–6908 (1992).
15. L. Changhai, X. Fengjie, H. Shengyang, and J. Zongfu, "Performance analysis of multiplexed phase computer-generated hologram for modal wavefront sensing," Appl. Opt. **50**, 1631–1639 (2011).
16. I. A. Litvin, A. Dudley, F. S. Roux, and A. Forbes, "Azimuthal decomposition with digital holograms," Opt. Express **20**, 10996–11004 (2012).
17. R. Borrego-Varillas, C. Romero, J. R. V. de Aldana, J. M. Bueno, and L. Roso, "Wavefront retrieval of amplified femtosecond beams by second-harmonic generation," Opt. Express **19**, 22851–22862 (2011).
18. T. Kaiser, D. Flamm, S. Schröter, and M. Duparré, "Complete modal decomposition for optical fibers using CGH-based correlation filters," Opt. Express **17**, 9347–9356 (2009).
19. D. Flamm, D. Naidoo, C. Schulze, A. Forbes, and M. Duparré, "Mode analysis with a spatial light modulator as a correlation filter," Opt. Lett. **37**, 2478–2480 (2012).
20. B. E. A. Saleh, M. C. Teich, *Fundamentals of Photonics* (Wiley, 1991)
21. J. W. Goodman, *Introduction to Fourier Optics* (McGraw-Hill Publishing Company, 1968).
22. M. Born and E. Wolf, *Principles of Optics* (Pergamon Press, 1991).
23. H. G. Berry, G. Gabrielse, and A. E. Livingston, "Measurement of the Stokes parameters of light," Appl. Opt. **16**, 3200–3205 (1977).
24. D. Flamm, O. A. Schmidt, C. Schulze, J. Borchardt, T. Kaiser, S. Schröter, and M. Duparré, "Measuring the spatial polarization distribution of multimode beams emerging from passive step-index large-mode-area fibers," Opt. Lett. **35**, 3429–3431 (2010).
25. B. Neubert and B. Eppich, "Influences on the beam propagation ratio M2," Opt. Commun. **250**, 241 – 251 (2005).
26. ISO, "ISO 15367-1:2003 lasers and laser-related equipment – test methods for determination of the shape of a laser beam wavefront – Part 1: Terminology and fundamental aspects," (2003).
27. R. T. Schermer, "Mode scalability in bent optical fibers," Opt. Express **15**, 15674–15701 (2007).
28. J. Leach, S. Keen, M. J. Padgett, C. Saunter, and G. D. Love, "Direct measurement of the skew angle of the poynting vector in a helically phased beam," Opt. Express **14**, 11919–11924 (2006).
29. F. A. Starikov, G. G. Kochemasov, S. M. Kulikov, A. N. Manachinsky, N. V. Maslov, A. V. Ogorodnikov, S. A. Sukharev, V. P. Aksenov, I. V. Izmailov, F. Y. Kanev, V. V. Atuchin, and I. S. Soldatenkov, "Wavefront reconstruction of an optical vortex by a Hartmann-Shack sensor," Opt. Lett. **32**, 2291–2293 (2007).

1. Introduction

Wavefront reconstruction of optical fields has become an important task in many domains of optics: astronomy, for example, is nowadays inconceivable without wavefront measurements. In combination with deformable mirrors for correction of distorted wavefronts, wavefront reconstruction has become a fundamental part of adaptive optics systems that enable high quality terrestrial observations [1]. Correction and control of wavefronts is no less essential in the fields of microscopy, such as 2-photon microscopy [2, 3] and confocal microscopy [4], and ophthalmology, such as optical coherence tomography [5] and scanning laser ophthalmoscopy [6]. Another field of application for wavefront control is laser material processing, in particular processes that require a high beam quality, such as laser cutting and drilling, often performed by fiber lasers [7, 8]. Concerning the wavefront measurement itself there exists a variety of different sensor types, including laser ray tracing [9], pyramid sensors [10], interferometric approaches [11–13] and the widely used Shack-Hartmann sensor (SHS) [14]. Recent advances have seen the use of computer-generated holograms (CGHs) to encode certain aberrations to determine the Zernike coefficients [15], the use of ring-shaped phase masks for decomposition in azimuthal modes [16], and non-linear approaches for high intensity light pulses [17].

In this work we focus on a new approach to wavefront and phase measurement based on the correlation filter method which makes use of an appropriate computer-generated hologram for complete modal decomposition of the light [18, 19]. In this method the laser beam under test illuminates the hologram, which performs the decomposition into a given set of modes (e.g.,

#171597 - $15.00 USD Received 29 Jun 2012; revised 2 Aug 2012; accepted 3 Aug 2012; published 13 Aug 2012

modes of a fiber or Laguerre-Gaussian modes of free space) due to a specific transmission function. In the far field diffraction pattern of the CGH, amplitudes and phases of these modes are measured yielding the complete information on the optical field. We extend this method and show that arbitrary optical fields can be reconstructed, including the accurate deduction of the mode content and the wavefront, and illustrate its robustness by measuring the phase and wavefront of a variety of laser beam classes, including vector beams and singular beams.

2. Modal decomposition

Modal decomposition is an elegant approach to characterize optical fields, where the measurement of a set of corresponding modal expansion coefficients yields amplitude and phase of the modes that compose the beam. While the concept is well known, only recently has it been shown to be viable in practical setups using the correlation filter method [18, 19]. For the benefit of the reader we briefly review the core concepts here. Physically, discrete modes appear in systems such as laser resonators and optical fibers, whereas shape and number of modes depend on the characteristics of the underlying system (e.g., resonator length or refractive index distribution of the fiber etc.). However, independent of the beam source, every optical field can be decomposed into a set of modes according to [18]:

$$\mathbf{U}(\mathbf{r}) = \sum_{l=1}^{N} c_l \Psi_l(\mathbf{r}), \tag{1}$$

with $\mathbf{r} = (x, y)$ the spatial coordinates, $c_l = \rho_l e^{i\Delta\varphi_l}$ the complex expansion coefficient, $\Psi_l(\mathbf{r}) = \psi_l(\mathbf{r})\mathbf{e}_l$ the l^{th} mode with amplitude ρ_l, intermodal phase differences $\Delta\varphi_l$ (phase difference between two modes, with one mode acting as a reference), polarization $\mathbf{e}_l$, and N the number of modes (which may count to infinity). Since the sum of the modes represents the entire optical field, the intensity and phase distributions of this field are easily computed via $I(\mathbf{r}) = |\mathbf{U}(\mathbf{r})|^2$ and $\Phi_j(\mathbf{r}) = \arg U_j(\mathbf{r})$ for each vector component U_j. To perform the modal decomposition into a given set of modes Ψ_l (for example modes of a fiber or Laguerre-Gaussian modes of free space) and to determine the set of coefficients c_l, as described by Eq. (1), is the main task of the correlation filter method. Note that the modes Ψ_l are calculated prior to any experiment and are thus known (an overview of the description of modes can be found in [20]). This enables the representation of the optical field $\mathbf{U}$ by a one-dimensional set of coefficients c_l, since the spatial information is stored in the modal fields ψ_l.

The centerpiece of the technique is a computer-generated hologram (CGH) that is illuminated by the beam. The diffraction pattern of the hologram is recorded in the far field and the amplitudes and phases of all modes are determined by measuring the intensity at the optical axis of the pattern, i.e., measuring the correlation signal of the incoming beam with the function inscribed in the hologram. This is the well-known measurement of the inner product (cf. [18,21]). The type of that transmission function depends on the quantity to be measured. Accordingly, to extract the amplitude of one specific mode, the transmission function is chosen to be the conjugate complex of the respective mode field [18, 21]:

$$T_l(\mathbf{r}) = \psi_l^*(\mathbf{r}), \tag{2}$$

where the asterisk denotes complex conjugation. Using this transmission function, the intensity on the optical axis in the Fourier plane is $I_l^{\rho} \propto \rho_l^2$, which is the power of mode ψ_l. To measure the intermodal phase difference $\Delta\varphi_l$ of a mode ψ_l to a chosen reference mode ψ_0 (mostly the fundamental mode, but in general arbitrary), two transmission functions are necessary, each representing an interferometric superposition of the two mode fields [18]:

$$T_l^{\cos}(\mathbf{r}) = [\psi_0^*(\mathbf{r}) + \psi_l^*(\mathbf{r})]/\sqrt{2}, \qquad T_l^{\sin}(\mathbf{r}) = [\psi_0^*(\mathbf{r}) + i\psi_l^*(\mathbf{r})]/\sqrt{2} \tag{3}$$

#171597 - $15.00 USD Received 29 Jun 2012; revised 2 Aug 2012; accepted 3 Aug 2012; published 13 Aug 2012

Again, from the correlation of the incoming field with the above transmission functions, resulting in intensities $I_l^{\sin} \propto \rho_0^2 + \rho_l^2 + 2\rho_0\rho_l \cos\Delta\varphi_l$ (corresponding to $T_l^{\sin}$) and $I_l^{\cos} \propto \rho_0^2 + \rho_l^2 + 2\rho_0\rho_l \sin\Delta\varphi_l$ (corresponding to $T_l^{\cos}$) on the optical axis in the Fourier plane, the intermodal phase difference $\Delta\varphi_l$ is calculated unambiguously according to [18]:

$$\Delta\varphi_l = -\arctan\left[\frac{2I_l^{\sin} - \rho_l^2 - \rho_0^2}{2I_l^{\cos} - \rho_l^2 - \rho_0^2}\right]. \tag{4}$$

To measure modal amplitudes ρ_l and phases $\Delta\varphi_l$ simultaneously from one diffraction pattern we use angular multiplexing. Accordingly, the final transmission function $T(\mathbf{r})$ of the hologram is a superposition of all single transmissions functions $T_n(\mathbf{r})$ (for each modal amplitude and sine and cosine of the phase), each modulated with a particular carrier frequency $\mathbf{K}_n$ to achieve spatial seperation of the information in the Fourier plane [18]:

$$T(\mathbf{r}) = \sum_{n=1}^{3N-2} T_n(\mathbf{r}) e^{i\mathbf{K}_n\mathbf{r}}. \tag{5}$$

Using the angular multiplexing, all amplitudes and phases can be measured simultaneously, enabling a high measurement rate of currently 30 Hz.

For scalar, i.e., linearly polarized beams, it is sufficient to image the beam plane of interest to the CGH. In the general case of arbitrarily polarized beams, a complete description of the optical field $\mathbf{U}$ is provided by the analysis of the cartesian field components U_x and U_y, including the proper phase difference δ between them. This can be done by measuring the Stokes parameters $S_0 \ldots S_3$ of the beam, which necessitates six (assuming completely polarized light) modal decompositions with a quarter-wave plate and a polarizer in appropriate orientations in front of the hologram [22, 23]:

$$\mathbf{S} = \begin{bmatrix} S_0 \\ S_1 \\ S_2 \\ S_3 \end{bmatrix} = \begin{bmatrix} |U_x|^2 + |U_y|^2 \\ |U_x|^2 - |U_y|^2 \\ 2|U_x||U_y|\cos\delta \\ 2|U_x||U_y|\sin\delta \end{bmatrix} = \begin{bmatrix} I(0^\circ) + I(90^\circ) \\ I(0^\circ) - I(90^\circ) \\ I(45^\circ) - I(135^\circ) \\ I_{\lambda/4}(45^\circ) - I_{\lambda/4}(135^\circ) \end{bmatrix}, \tag{6}$$

where $I(\alpha)$ is the measured (respectively reconstructed) intensity behind the polarizer at angular orientations $\alpha = 0^\circ$, 45°, 90°, 135° and $I_{\lambda/4}(\alpha)$ denotes two additional measurements with the polarizer placed at $\alpha = 45^\circ$, 135° and a preceding quarter-wave plate. Having performed the depicted six modal decompositions, the optical field, including the polarization properties, is completely known [24].

3. Wavefront reconstruction

As mentioned in the previous section, the entire optical field is accessible using a CGH in combination with standard polarization optical components. This equally means that the Poynting vector $\mathbf{P}$ is computable from [22]:

$$\mathbf{P}(\mathbf{r}) = \frac{1}{2}\Re[\mathbf{E}(\mathbf{r}) \times \mathbf{H}^*(\mathbf{r})] = \frac{1}{2}\Re\left[\frac{i}{\omega\varepsilon_0}\varepsilon^{-1}(\mathbf{r})[\nabla \times \mathbf{U}(\mathbf{r})] \times \mathbf{U}^*(\mathbf{r})\right], \tag{7}$$

where ω is the angular frequency, ε_0 the vacuum permittivity, ε the permittivity distribution, and $\mathbf{E}$ and $\mathbf{H}$ are the electric and magnetic field respectively, that both obey the decomposition of Eq. (1). On the right-hand side of Eq. (7), $\mathbf{H}$ was assumed to be the vector field $\mathbf{U}$, and $\mathbf{E}$ was calculated according to Maxwell's Equations. Note that alternatively the vector field could

#171597 - $15.00 USD Received 29 Jun 2012; revised 2 Aug 2012; accepted 3 Aug 2012; published 13 Aug 2012

have been chosen to be the electric field, which yields the same Poynting vector. The wavefront is then usually defined as the continuous surface that is normal to the time average direction of energy propagation, i.e., normal to the time average Poynting vector $\mathbf{P}$ [25, 26]:

$$w(\mathbf{r},z) \perp \mathbf{P}(\mathbf{r},z), \tag{8}$$

where z denotes the position of the measurement plane. Since there might be no continuous surface that fulfills this condition, the wavefront can be more generally defined as the continuous surface that minimizes the power density weighted deviations of the direction of its normal vectors to the direction of energy flow in the measurement plane [25, 26]:

$$\int\int |\mathbf{P}| \left| \frac{\mathbf{P}_t}{|\mathbf{P}|} - \nabla_t w \right|^2 dA \rightarrow \min, \tag{9}$$

where $\mathbf{P}_t = [P_x, P_y, 0]'$. In the simple case of scalar, i.e. linearly polarized, beams the wavefront is equal to the phase distribution $\Phi(\mathbf{r})$ of the beam, except for a proportionality factor [26]:

$$w(\mathbf{r}) = \frac{\lambda}{2\pi}\Phi(\mathbf{r}). \tag{10}$$

It is important to note that this expression is only valid as long as there are no phase jumps or phase singularities, because the wavefront is always considered to be a continuous surface.

4. Measurement setup

The experimental setup as schematized in Fig. 1 consisted of a beam source (for example a laser resonator or an optical fiber) to generate an aberrated wavefront, and the analyzing system, comprised of the modal decomposition branch, including CGH and two cameras, and an optional Shack-Hartmann sensor (SHS) for comparison of results. To decompose the optical field with the aberrated wavefront into a well defined set of modes regarding number and size, as well as to achieve arbitrary mode superpositions and polarization properties, the beam source was chosen to be an optical step-index fiber (core diameter 7.7 μm) in the first instance, excited with a Nd:YAG laser (λ =1064 nm) and guiding three fiber modes. Hence, the aberrated wavefront was generated at the fiber end face by multimode interference. The reliability of the modal decomposition approach was proved by comparing the results to those of a Shack-Hartmann wavefront sensor. A beam splitter (non-polarizing) was used to analyze the beam with the wavefront sensor and with the modal decomposition setup at the same time. Two different 4f-setups with magnifications of $f_{\mathrm{L3}}/f_{\mathrm{L1}} = 750\,\mathrm{mm}/4\,\mathrm{mm} = 188$ and $f_{\mathrm{L2}}/f_{\mathrm{L1}} = 375\,\mathrm{mm}/4\,\mathrm{mm} = 94$, respectively, relay imaged the plane of the aberrated wavefront (here end face of the respective fiber) to the wavefront sensor and to the CGH (cf. Fig. 1), with the focal lengths chosen that first, the beam matched the design radius of the hologram, and second, the beam was well sampled by the microlens array of the wavefront sensor. The wavefront sensor consisted of 69×69 microlenses with an array pitch of 0.108 mm. Via a second beam splitter (non-polarizing), the fiber end face was simultaneously imaged onto the CGH and a CCD camera for direct recording of the near field intensity (CCD_1, cf. Fig. 1). Thereby, a polarizer and an optional quarter-wave plate were used to perform the Stokes measurements, whereas the CGH performed the modal decomposition for each polarization component. The hologram diffraction pattern of first order was observed with a second CCD camera (CCD_2) in the far field of the hologram using a single lens in a 2f-setup ($f_{\mathrm{FL}} = 180\,\mathrm{mm}$), and was used to determine the modal powers and phases of the beam for the scalar projection provided by the pair of quarter-wave plate and polarizer. Note that for a linearly polarized beam, quarter-wave plate and polarizer would not have been necessary. The hologram itself was written to either a commercial pixelated phase-only spatial

#171597 - $15.00 USD Received 29 Jun 2012; revised 2 Aug 2012; accepted 3 Aug 2012; published 13 Aug 2012

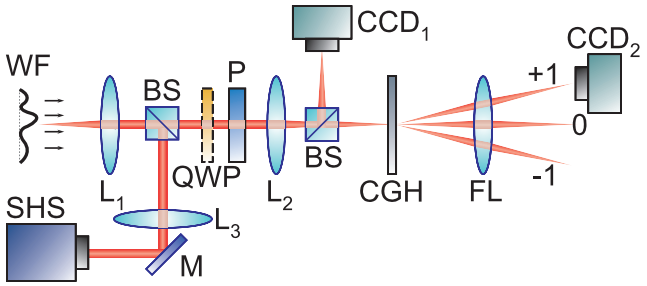

Fig. 1. Scheme of the measurement setup: WF aberrated wavefront to be relay imaged onto the computer-generated hologram (CGH) and the Shack-Hartmann wavefront sensor (SHS), MO microscope objectives, QWP quarter-wave, P polarizer, $L_{1,2,3}$ lenses, FL Fourier lens, BS beam splitter, $CCD_{1,2}$ CCD cameras, M mirror.

light modulator (SLM, Holoeye Pluto) [19] or a customized pixelated solid amplitude-only filter fabricated via laser lithography [18]. Both methods are shown to yield accurate results in the following.

5. Calibration of the setup

To ensure that both measured wavefronts, from modal decomposition and Shack-Hartmann measurement, are solely created by the fiber beam itself and not influenced by the optical setup (lenses, beam splitters, etc.) some kind of calibration is necessary. To avoid impact of especially defocus and to ensure proper imaging of the plane of the fiber end facet to wavefront sensor and CGH, the focal length of each used lens was measured with the wavefront sensor, entering the lenses with a collimating beam and using the Zernike coefficient of defocus to determine the focal length and principal plane. Placing the lenses at the proper distances the experimental setup as a whole was calibrated using the fundamental mode of the fiber, which has a flat wavefront. Accordingly, the setup was adjusted to result in a wavefront as flat as possible in the detection planes. A pure fundamental mode beam at the fiber end face was guaranteed by strong fiber bending, which causes all possibly excited higher order modes to experience severe losses [27]. Fundamental mode illumination on the CGH is used as well to define the optical axis and to align the hologram. The outcome of this procedure is shown for one example in Fig. 2. Figure 2(a) and (c) depict the measurement results of the Shack-Hartmann wavefront sensor. As can be seen, the recorded wavefront is very flat with a maximum deviation from the plane below 0.09 μm, which is less than $\lambda/10$. Additionally, the intensities measured with the wavefront sensor (Fig. 2(a)) and with the CCD camera (Fig. 2(b)) are in good agreement, which is, alongside with the flat wavefront, another proof that the optical setup itself adds no severe aberrations. The modal decomposition results in a modal spectrum (Fig. 2(d)) with a fundamental mode power of 99% of total power, which demonstrates the pureness of the reference beam.

6. Scalar beams

After aligning the hologram and the wavefront sensor with the fundamental mode, the position of the fiber seed beam with respect to the fiber front face was shifted to excite some higher order modes in the fiber. The experiments were done with a step-index fiber with core diameter of 7.7 μm and a numerical aperture of 0.12. Hence, the fiber guides three modes at 1064 nm. As the CGH we used a solid amplitude-only diffractive device, fabricated via laser lithography,

#171597 - $15.00 USD Received 29 Jun 2012; revised 2 Aug 2012; accepted 3 Aug 2012; published 13 Aug 2012

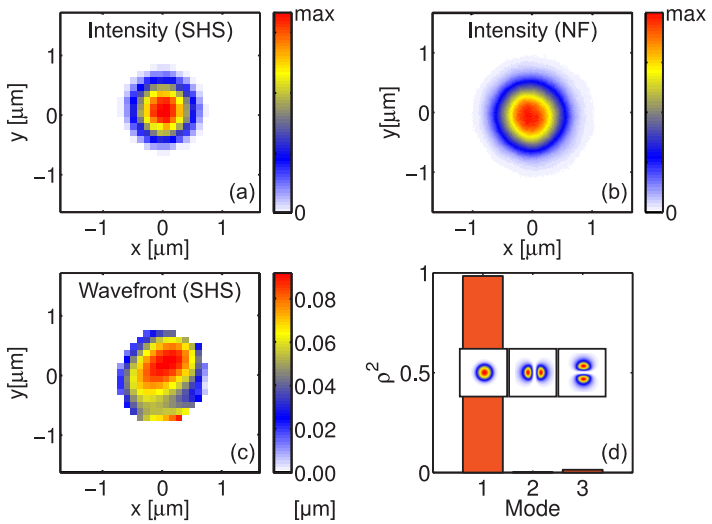

Fig. 2. Fundamental mode illumination of CGH and wavefront sensor for calibration. (a) Intensity measured with the wavefront sensor. (b) Intensity measured with the CCD camera. (c) Wavefront measured with the wavefront sensor (scale in μm). (d) Modal power spectrum (insets depict respective mode intensities).

for all fiber experiments [18]. To perform scalar experiments a polarizer was placed between the fiber end face and the first beam splitter that divides the beam for analysis with CGH and wavefront sensor. This procedure enables the reconstruction of the wavefront from the phase as described by Eq. 10, which is beneficial because no measurement of Stokes parameters is necessary. In this way, we reconstructed the wavefront with up to 30 Hz using the CGH, only limited by the maximum camera frame rate.

Figure 3 depicts the results for a fiber beam with higher order mode content. According to the measured modal power spectrum (Fig. 3(c)) the beam consists of 44% fundamental mode, 18% mode 2 and 38% mode 3 (modal intensities depicted in insets of Fig. 3). Figure 3(a) and (b) show with wavefront sensor measured intensity and from the modal decomposition reconstructed intensity (according to Eq. (1)). Both intensities are in good agreement, which indicates the absence of setup induced aberrations and proves the reliability of the modal decomposition. The wavefront of the beam is measured with the Shack-Hartmann sensor (Fig. 3(d)) and using the modal decomposition approach. In the latter case, for the scalar beam under test, both reconstruction options, from phase (Eq. (10), Fig. 3(e)) and minimization (Eq. (9), Fig. 3(f)) are demonstrated. All wavefront results are in good agreement concerning shape and scale. Obviously in this case where there are no phase jumps or singularities, Eq. (10) is valid for wavefront reconstruction. Since aberrations possibly added by the optical setup would have given rise to deviations in the wavefronts, significant influence of these aberrations can be excluded. Note that a wavefront reconstruction using the CGH could not incorporate such aberrations, when the decomposition is done in fiber modes only. As a consequence, only aberrations emerging from mode superpositions itself can be detected in that case (cf. section 9 for a more general approach). Additionally, it is important to notice that the wavefront reconstructed with the CGH (Fig. 3(e) and (f)) is artificially truncated to values where the corresponding intensity exceeds 5% of its maximum value, to enable better comparison with the Shack-Hartmann measurement. Actually, using the CGH, wavefront and phase are reconstructed in the entire frame and are not restricted to the depicted area.

#171597 - $15.00 USD Received 29 Jun 2012; revised 2 Aug 2012; accepted 3 Aug 2012; published 13 Aug 2012

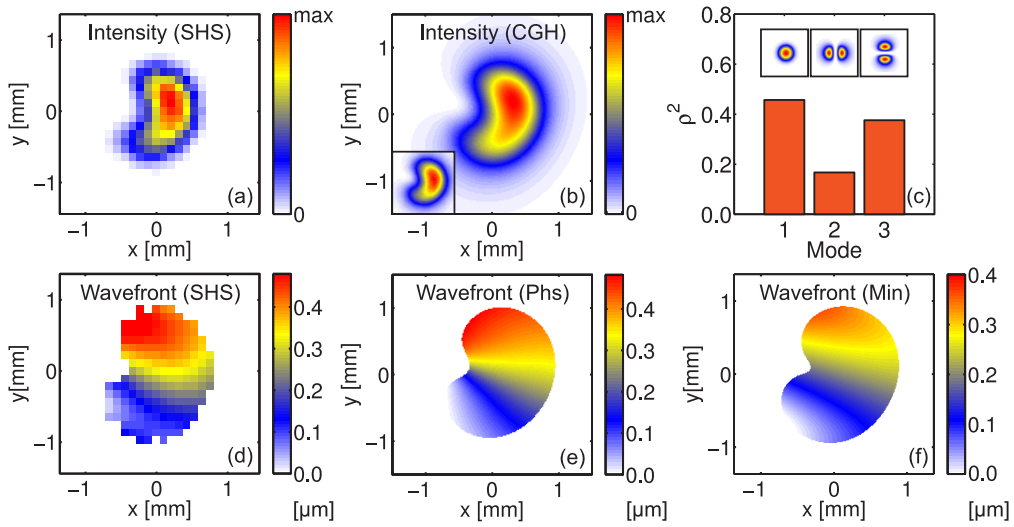

Fig. 3. Wavefront reconstruction for a higher order mode scalar beam. (a) Intensity measured with the wavefront sensor (SHS). (b) Reconstructed intensity (inset depicts directly measured intensity with CCD_1). (c) Modal power spectrum (insets depict mode intensities). (d) Wavefront measured with the Shack-Hartmann sensor (scale in μm). (e) Wavefront determined from the phase reconstruction according to Eq. (10) (scale in μm). (f) Wavefront from the minimization according to Eq. (9) (scale in μm).

7. Vector beams

To reconstruct vector beams, i.e., beams with in general spatially varying polarization, requires a higher number of CGH-measurements. To incorporate the vector nature of the beam, the polarization properties need to be determined to correctly reconstruct the wavefront. This is done by a combination of a classical measurement of Stokes parameters and a modal decomposition with the CGH. Thereby the knowledge of polarization properties accompanied with the modal information completely characterizes the vector field [24]. The experiment is performed by placing a quarter-wave plate and a polarizer in front of the hologram and performing six modal decompositions according to Eq. (6). This yields the field components U_x and U_y as well as their relative phase difference δ and hence, the entire optical field, including the Poynting vector $\mathbf{P}$. The wavefront w is infered according to Eq. (9) by numerically minimizing the direction deviations of Poynting vector and wavefront normal vectors, weighted with the power density $|\mathbf{P}|$. Results of this procedure are depicted in Fig. 4. In this example, the beam consists of 63% fundamental mode, 23% mode 2 and 14% mode 3 as shown in Fig. 4(c) (modal powers of x- and y-component added up). As seen from the intensity plots Fig. 4(a) and (b), the beam is shifted slightly off-axis due to modal interference. Measured intensities from both the Shack-Hartmann (Fig. 4(a)) and the CGH reconstruction (Fig. 4(b)) are in very good agreement. Regarding the wavefronts, results from direct Shack-Hartmann measurement (Fig. 4(d)) and from minimization based on Eq. (9) (Fig. 4(f)) correlate very well. However, since there is no phase of the entire vector field (each component has its own phase) in this case, there is no way to determine the wavefront according to Eq. (10).

#171597 - $15.00 USD Received 29 Jun 2012; revised 2 Aug 2012; accepted 3 Aug 2012; published 13 Aug 2012

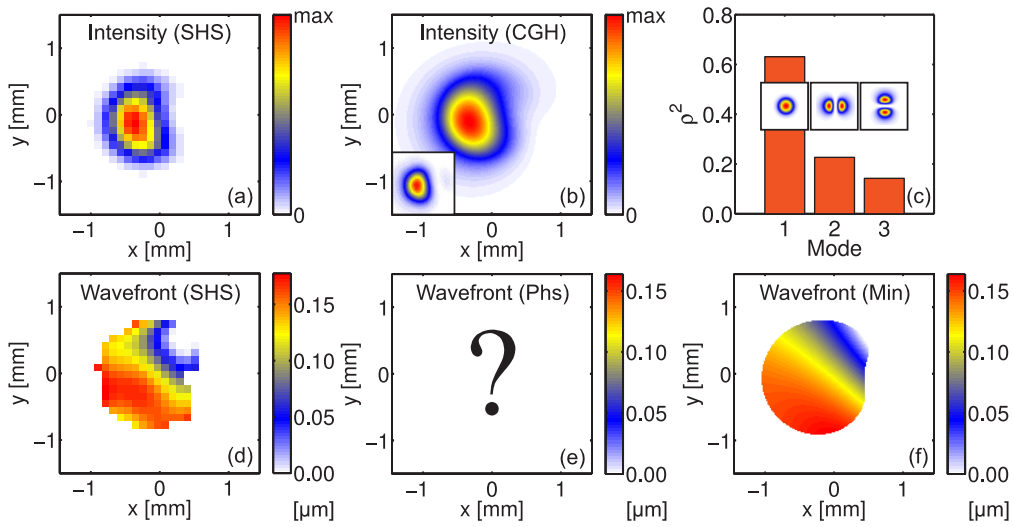

Fig. 4. Wavefront reconstruction for a higher order mode non-scalar beam. (a) Intensity measured with the wavefront sensor (SHS). (b) Reconstructed intensity (inset depicts directly measured intensity with CCD_1). (c) Modal power spectrum. (d) Wavefront measured with the Shack-Hartmann sensor (scale in μm). (e) Phase distribution is not well defined. (f) Wavefront from the minimization according to Eq. (9).

8. Beams with phase singularities

It is pertinent to apply the technique to singular beams: beams containing optical vortices. An interesting example of a such a beam is a scalar donut beam, because of its exceptional phase distribution. Such a donut beam is formed by a coherent superposition of the two higher order fiber modes (cf. insets of Fig. 5(c)), each with nearly equal content and a relative phase difference of $\pi/2$. The fundamental mode is absent in this special case. The described superposition forms a phase singularity in the center of the beam with a corresponding zero intensity point.

Results for such a superposition are depicted in Fig. 5. The illustrated example was achieved by tuning excitation position of the seed laser with respect to the fiber, mostly to obtain equal power of the higher order modes and zero power for the fundamental. The relative phase difference necessary to create the ring-shape at the fiber output was tuned by bending the fiber. Again, the intensity distributions recorded with Shack-Hartmann sensor and reconstructed with the CGH are depicted in Fig. 5(a) and (b), next to the modal power spectrum Fig. 5(c), revealing nearly equal power in mode 2 and 3. The interesting part is now to compare the wavefront results (Fig. 5(d)-(f)). Since the example depicts a scalar beam with a well defined phase distribution, it is tempting to infer the wavefront according to Eq. (10). As expected the phase distribution, and following Eq. (10) also the wavefront, is a spiral with a singularity in its center (Fig. 5(e)). However, comparing this result to those achieved by the Shack-Hartmann sensor (Fig. 5(d)) and the reconstruction from minimization (Fig. 5(f)), it appears that both wavefronts are flat ($w_{\mathrm{max}} < 0.1\,\mu$m). This deviance is actually based on the problem of defining the wavefront as a physical quantity itself. Other than the phase, the wavefront is connected to the Poynting vector [26]. It is known that the Poynting vector spirals for a vortex beam [28], so one might expected a spiralling wavefront too. On the other hand, the definition according to the ISO-standard defines the wavefront as a continuous surface, which excludes jumps and singularities [26]. Considering a surface perpendicular to the direction of the Poynting vector, it becomes obvious that no continuous surface exists that fulfills that condition, even though

#171597 - $15.00 USD Received 29 Jun 2012; revised 2 Aug 2012; accepted 3 Aug 2012; published 13 Aug 2012

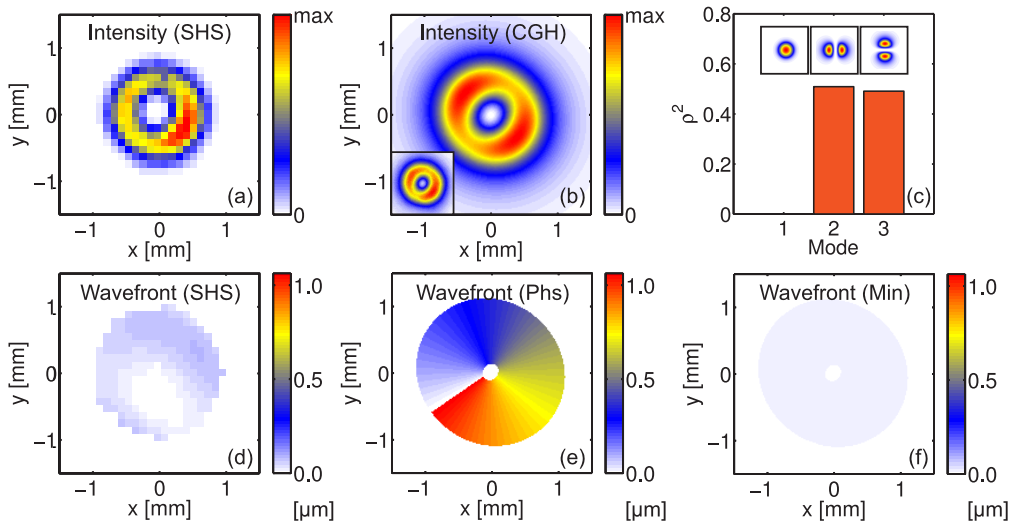

Fig. 5. Wavefront reconstruction for a scalar donut beam. (a) Intensity measured with the wavefront sensor (SHS). (b) Reconstructed intensity (inset depicts directly measured intensity with CCD_1). (c) Modal power spectrum. (d) Wavefront measured with the Shack-Hartmann sensor (scale in μm). (e) Wavefront determined from the phase reconstruction (scale in μm). (f) Wavefront from the minimization according to Eq. (9).

the Poynting vector spirals continuously. Accordingly, the only continuous surface, that minimizes the integral in Eq. (9), is a flat surface. Instead of pretending that this surface has a physical reality, one must argue that in the case of a vortex beam, the wavefront is not well defined. However, the phase distribution is defined and is easily reconstructed revealing the helical structure. Hence, it is redundant to ask for a wavefront since the optical field is known by the modal decomposition and no additional information is achieved by asking for a wavefront. So, this example nicely reveals the difference between phase (here spiral) and wavefront (here flat) of a beam, which are often equal in shape, but which are in fact two different physical quantities [25]. This discrepancy has been pointed out by others using the Shack-Hartmann approach to measure wavefronts of vortex beams [29].

9. Decomposing beams including extrinsic aberrations

As discussed earlier, decomposing a fiber beam into its modal components is beneficial because of the well defined number and scale of the modes in that case. However, the reconstruction of aberrations is limited to those that arise from multimode interference of individual fiber modes only, since the set is constrained to a certain number and adapted to the fiber geometry. The most general case of reconstructing arbitrary aberrations is done by decomposing into a set of free space modes, as Hermite-Gaussian or Laguerre-Gaussian modes. The benefit of universality is payed dearly for the large number of modes that might be necessary, since in constrast to the fiber mode set, the free space mode set is mathematically complete only with an infinite number of modes. However, from a practical point of view a truncation to a reasonable number, depending on the complexity of the contained aberrations, can always be found. To demonstrate the principle, the optical fiber was replaced by a helium-neon laser emitting a fundamental Gaussian beam, which was externally aberrated on purpose. For convenience, we chose the aberration to be defocus, easily achieved by letting the beam pass a positive lens. The plane of the lens was 4f-imaged onto the CGH to decompose the aberrated beam. The hologram was

#171597 - $15.00 USD Received 29 Jun 2012; revised 2 Aug 2012; accepted 3 Aug 2012; published 13 Aug 2012

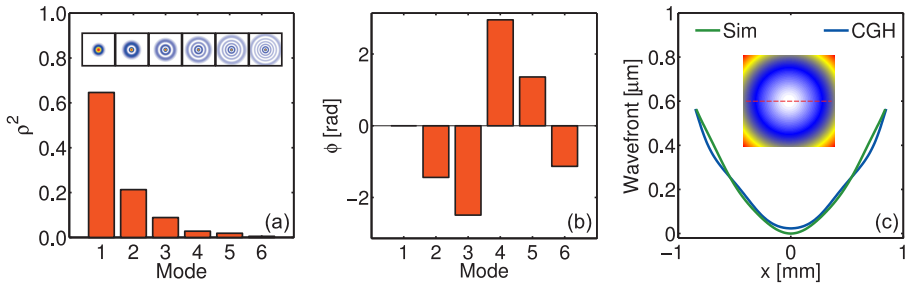

Fig. 6. Wavefront reconstruction of a fundamental Gaussian beam with extrinsically added wavefront curvature using a lens of focal length $f = 1000\,\mathrm{mm}$. (a) Modal power spectrum (insets depict Laguerre Gaussian modes LG_{p0} used for decomposition). (b) Intermodal phase differences. (c) Comparison of reconstructed (CGH) and theoretically expected (Sim) wavefront (cross section through center). The inset in (c) depicts the measured two-dimensional wavefront (same scale as (c)). See Media 1 for the decay of higher order mode signal in the diffraction pattern of the hologram, and Media 2 for the corresponding hologram phase pattern, both for a lens of $f = 500\,\mathrm{mm}$.

now implemented using a phase-only spatial light modulator (SLM) to attain more flexibility regarding the properties of the mode set (number, size, curvature) [19].

Results are shown in Fig. 6 for a lens of 1000 mm focal length. Adding a wavefront curvature onto the field by means of the lens results in a modal spectrum with higher order mode content, which decays towards higher orders. These higher order modes are, in combination with the saw-tooth shaped modal phase pattern, necessary to reconstruct the field with curved wavefront. Note that only LG_{p0} modes respond in case of pure defocus. The good agreement between the expected wavefront for a lens with focal length $f = 1000\,\mathrm{mm}$ and the measured one is emphasized in Fig. 6(c), depicting a wavefront slice through the center. Another proof of accuracy for the measured wavefront is to incorporate the conjugated curvature into the modal basis set and running the decomposition again, easily achieved by changing the hologram on the SLM. This time, as shown in Fig. 7(b), the modal spectrum consists to 99% of fundamental mode. Since the conjugate of the measured curvature is already included in each mode on the hologram, this procedure yields a perfectly adapted mode set and consequently a response of the fundamental mode only. Or in other words, the curvature of the physical lens is balanced by the conjugated curvature programmed on the hologram. Hence, the modal spectrum resembles that of a modal decomposition performed without a physical lens in place and into modes with a flat wavefront, as illustrated in Fig. 7(a).

10. Discussion of techniques

The two wavefront measurement techniques using a Shack-Hartmann sensor and a computer-generated hologram are very different in their physical approach to reconstruct the wavefront. Whereas the Shack-Hartmann sensor deduces the wavefront from the foci positions of the microlenses and therewith from the wavefront slope, the CGH-technique provides a modal decomposition of the beam, yielding the complete information about the optical field, from which the wavefront can be deduced by Eq. (9) or Eq. (10). This great difference in strategy is equally reason for a number of advantages and disadvantages.

In view of the measurement rate both techniques are very similar with maximum rates of 30 Hz (limited by the frame rate of the camera). On the contrary, in case of inhomogeneously polarized beams the wavefront reconstruction with the CGH takes roughly a minute, caused by the Stokes measurement and the running time of the minimization routine. On the other hand,

#171597 - $15.00 USD Received 29 Jun 2012; revised 2 Aug 2012; accepted 3 Aug 2012; published 13 Aug 2012

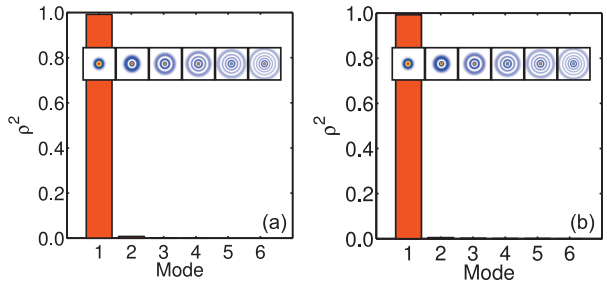

Fig. 7. (a) Modal decomposition without physical lens and decomposition into modes without curvature. (b) Modal decomposition into modes that incorporate the wavefront curvature measured in Fig. 6 for a physical lens $f = 1000\,\mathrm{mm}$. The insets depict the corresponding mode intensities.

the wavefront reconstruction using a CGH is very beneficial for some reasons. One is the spatial resolution: whereas the Shack-Hartmann sensor is very limited in resolution by the number of microlenses, the resolution of the wavefront determined by the CGH has no theoretical limit. Since the directly measured values (modal powers and phases) are scalar numbers, the resolution from a practical point of view is given by the number of pixels per unit length with which the modal fields can be calculated. A second advantage is the extension of the measurement area of the wavefront. Regarding the Shack-Hartmann sensor it is immediately clear that the wavefront cannnot be measured at points where there is little or no intensity, as for example at phase singularities. Of course this is also limiting for the minimization of the integral in Eq. (9). In contrast, the phase of the beam, as determined by the CGH, is defined everywhere, i.e., also in regions with no intensity. Another issue is represented by the measurable wavefront slope. The slope limit for the Shack-Hartmann sensor is given by the case where the focus of one microlens is shifted to the evaluation area of an adjacent lens. Concerning the reconstruction with the CGH there is no theoretical limit regarding the wavefront slope, e.g., phase jumps are easily detected.

11. Conclusion

In conclusion, we presented a new method to reconstruct wavefronts based on modal decomposition using computer-generated holograms. We have illiustrated the power of the method by reconstructing wavefronts from both fiber and free space modes by a modal decomposition of the field. The versatility of the approach was demonstrated by studying arbitrary mode superpositions, complex polarization properties, vortex beams and aberrated Gaussian beams. Different reconstruction options were outlined, such as reconstructing the wavefront from the phase distribution for scalar beams without phase singularities and jumps, and reconstruction from the Poynting vector for the general case of inhomogeneously polarized beams. Our results were validated by comparison with Shack-Hartmann measurements. Pros and cons of wavefront reconstructions based on modal decomposition with respect to Shack-Hartmann measurements were discussed regarding applicability, measurement rate, spatial resolution, area of measurement, and measurable wavefront slope. The most striking advantages of our method is seen in spatial resolution, area of measurement, and measurable slope.

Acknowledgments

The authors would like to thank Mr. B. Eppich for the productive discussions and valueable hints and ideas.

#171597 - $15.00 USD Received 29 Jun 2012; revised 2 Aug 2012; accepted 3 Aug 2012; published 13 Aug 2012